



CHORUS

This is the accepted manuscript made available via CHORUS. The article has been published as:

Evaluation of exchange-correlation functionals with multiple-shock conductivity measurements in hydrogen and deuterium at the molecular-to-atomic transition

M. D. Knudson, M. P. Desjarlais, M. Preising, and R. Redmer

Phys. Rev. B **98**, 174110 — Published 26 November 2018

DOI: [10.1103/PhysRevB.98.174110](https://doi.org/10.1103/PhysRevB.98.174110)

Abstract

The temperature (T) and density (ρ) conditions at which hydrogen undergoes a molecular-to-atomic (MA) transition is crucial to our understanding of the gas-giant planets such as Jupiter and Saturn. First-principles (FP) calculations suggest that this transition is coincident with metallization and acts as a catalyst for hydrogen-helium demixing, which has significant consequences for models of planetary interiors. Prediction of this transition boundary has proven to be difficult using FP methods. In particular, detailed comparisons of finite temperature density functional theory (FT-DFT) calculations of the MA transition in both the high- T , low- ρ regime, where the transition is largely T -driven, and the low- T , high- ρ regime, where the transition is largely ρ -driven, suggest that the transition is very sensitive to the exchange-correlation (xc) functional used in the calculation. Here we present a detailed comparison of previous multiple-shock electrical conductivity measurements with FT-DFT calculations employing various xc functionals to probe a regime where both T and ρ play an important role in the transition. The measurement results are found to be inconsistent with the semi-local xc functional PBE, and are in much better agreement with the nonlocal xc functionals vdW-DF1 and vdW-DF2. Furthermore, we show that the inconsistency with PBE likely stems from pressure errors associated with the PBE xc functional, resulting in calculated pressures that are too low at these T and ρ conditions. Together with previous comparisons at high- T , low- ρ and low- T , high- ρ these results provide a consistent picture for the MA transition over a wide T and ρ range. This picture may also provide insight into differences in experimental observations of the metallization of liquid hydrogen and deuterium in the low- T regime.

10 I. INTRODUCTION

11 The question of precisely how and at what pressure (P) hydrogen metallizes at low
12 temperature (T) has become one of the longest-standing open questions of high-pressure
13 physics.¹ Also of great interest, due to its relevance to planetary science,^{2,3} is the analo-
14 gous molecular insulator to atomic metal transition in the liquid at low T , just above the
15 melt boundary. First-principles (FP) calculations suggest that hydrogen metallization is
16 coincident with a molecular-to-atomic (MA) transition and acts as a catalyst for hydrogen-
17 helium demixing.⁴ Thus the location of the MA transition in the low- T liquid could provide
18 a constraint for the low- P boundary of the region of hydrogen-helium immiscibility and
19 justification for the presence of a layer boundary in the interior of gas-giant planets, a nec-
20 essary feature of the often-used three-layer model,⁵ which has shown reasonable success in
21 describing observables of Jupiter and Saturn.⁶

22 Hydrogen, as one of the simplest elemental systems, has also been a model system in
23 the development of advanced FP simulation techniques including finite temperature density
24 functional theory (FT-DFT) and quantum Monte Carlo (QMC) methods.¹ However, predic-
25 tion of the MA transition using FP methods has proven to be very sensitive to the framework
26 used. Recent work⁷ comparing FT-DFT methods to the deuterium Hugoniot – the locus
27 of end states achievable through compression by large amplitude shock waves – concluded
28 that no one exchange-correlation (xc) functional adequately describes the MA transition. In
29 this high- T (~ 5 -10 kK), low-density (ρ) regime where dissociation is largely T -driven the
30 P onset of the MA transition, as evidenced by first-shock ρ and reshock P measurements,
31 is underestimated by the semi-local xc functional PBE⁸ and is best described by nonlocal
32 functionals, such as vdW-DF1⁹ and vdW-DF2.¹⁰ However, the P width over which disso-
33 ciation occurs is likely overestimated by these vdW functionals, and is in better agreement
34 with PBE.

35 Differences between functionals become even more pronounced in the low- T (~ 1 -2 kK),
36 high- ρ regime where the MA transition appears to be largely ρ -driven. In this regime the
37 predicted transition P and ρ are extremely sensitive to the xc functional. For PBE, vdW-
38 DF1, and vdW-DF2 the predicted transition P differs by ~ 200 -300 GPa (see Fig. 1) and
39 the ρ at the transition ranges from ~ 0.75 -1.2 g/cm³ for hydrogen and ~ 1.5 -2.4 g/cm³ for
40 deuterium.¹¹⁻¹⁵ Experimental determination of the MA transition in this regime also span a

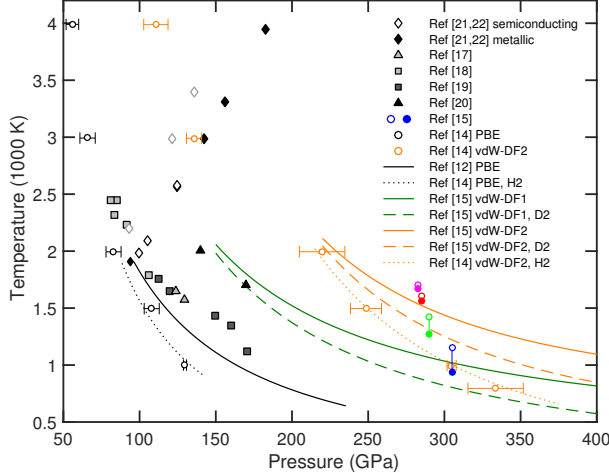


FIG. 1. T - P phase diagram showing experimental and theoretical estimates for the metallization of hydrogen/deuterium. Experiment: open (closed) diamonds,^{21,22} semiconducting (metallic) states from multiple-shock experiments with corrected T (see Sec. II); gray triangle,¹⁷ gray square,¹⁸ black square,¹⁹ and black triangle,²⁰ static high- P and pulsed heated experiments; colored open and closed circles,¹⁵ dynamic compression experiments. Theory: open black (orange) circles,¹⁴ calculations of $\sigma = 2000$ (Ω cm)⁻¹ for PBE (vdW-DF2) with nuclear (hydrogen) treatment for the ions; solid¹² and dotted¹⁴ black lines, first-order MA transition boundary for PBE with classical and nuclear (hydrogen) treatment for the ions, respectively; solid and dashed green lines,¹⁵ transition boundary for vdW-DF1 with classical and nuclear (deuterium) treatment for the ions, respectively; solid,¹⁵ dotted,¹⁴ and dashed¹⁵ orange lines, transition boundary for vdW-DF2 with classical, nuclear (hydrogen), and nuclear (deuterium) treatment of the ions, respectively.

41 large range in P . Dynamic compression experiments¹⁵ on liquid deuterium in the ~ 1 -2 kK
 42 regime performed at the Sandia Z machine¹⁶ revealed an abrupt MA transition, as evidenced
 43 by a sudden increase in reflectivity between ~ 280 and 305 GPa, in reasonable agreement
 44 with the nonlocal vdW-DF2 xc functional. Static high- P and pulsed heated experiments¹⁷⁻²⁰
 45 on hydrogen and deuterium in a similar T regime suggest the MA transition occurs at ~ 75
 46 to 170 GPa, based on observation of T plateaus in the heating curves and increases in
 47 reflectivity, seemingly in better agreement with the semi-local xc functional PBE.

48 The first experiments^{21,22} to address the MA transition in liquid hydrogen and deuterium
 49 were performed roughly 20 years ago using gas-gun techniques. In that study multiple-
 50 shock compression, achieved through a wave reverberation technique, was used to attain

51 successively higher P and T states in liquid hydrogen and deuterium. Measurement of the
 52 electrical conductivity (σ) in the peak state revealed saturation at ~ 2000 ($\Omega \text{ cm}$)⁻¹, a value
 53 consistent with minimum metallic conductivity, at a P of ~ 140 GPa and an estimated T
 54 of ~ 2600 K. This set of experiments provides another very good test of FP methods in a
 55 regime in which both T and ρ (or P) play an important role in the MA transition. However,
 56 while indirect comparisons between the measured σ and FP calculations have been made, to
 57 the best of our knowledge no one has performed a detailed comparison of these experimental
 58 results with FP calculations.

59 Here we present a detailed comparison of the measured σ from multiple-shock compression
 60 experiments^{21,22} with FT-DFT calculations using both semi-local (PBE) and nonlocal (vdW-
 61 DF1 and vdW-DF2) xc functionals. We show that the measured results are inconsistent
 62 with PBE predictions. Similar to both the T -driven and ρ -driven regime, PBE appears to
 63 underestimate the P conditions necessary for dissociation. In contrast, the MA transition
 64 appears to be better described by the vdW xc functionals. Furthermore, we show that the
 65 inconsistency with PBE likely stems from P errors associated with the PBE xc functional,
 66 resulting in calculated P that are too low at these T and ρ conditions. These results,
 67 along with the previous studies comparing the various xc functionals in the T -driven⁷ and
 68 ρ -driven¹⁵ regimes, provide a consistent picture for the MA transition over a wide P and
 69 T range, and raise questions about the recent static high- P and pulsed heated studies¹⁷⁻²⁰
 70 that appear to be in agreement with predictions from PBE.

71 Section II summarizes the multiple-shock experiments,^{21,22} and includes a reanalysis of
 72 the results. The original study included inconsistencies in both the inferred T states reached
 73 and in the fit to a semiconductor model used to interpret the measured σ . Correction of both
 74 of these inconsistencies is important with respect to comparisons with the FP calculations.
 75 Section III describes the FT-DFT calculations performed to determine σ and the energy
 76 gap for the various xc functionals and compares these with the experimental measurements.
 77 The results are discussed in Sec. IV. The main findings are summarized in Sec. V.

78 II. REANALYSIS OF MULTIPLE-SHOCK CONDUCTIVITY EXPERIMENTS

79 The first experiments^{21,22} to address the MA transition in hydrogen and deuterium were
 80 performed roughly 20 years ago by Nellis, Weir, and Mitchell (NWM) using gas-gun tech-

81 niques. A layer of liquid hydrogen or deuterium was compressed by multiple-shocks using
82 a wave reverberation technique; this minimized the entropy increase, thereby minimizing
83 the temperature (T) in the peak state. The sample was contained within a cell between
84 two sapphire anvils and cooled to cryogenic temperatures. The sample cell was impacted
85 by a metal anvil (either aluminum or copper) resulting in a strong shock wave that rever-
86 berated between the relatively stiff sapphire anvils, driving the sample to high pressure (P)
87 and density (ρ) and relatively low T . The impact velocity (v_f) was measured using a flash
88 x-ray technique.²³ The peak P of the sample was determined from the known equations of
89 state (EOS) of aluminum, copper, and sapphire and the measured v_f (in the reverberation
90 configuration the peak P is only a function of the confining anvils and does not depend
91 upon the EOS of hydrogen or deuterium). The electrical conductivity (σ) was measured at
92 the peak state using either a constant-voltage, two-probe method ($\sigma < 10 (\Omega \text{ cm})^{-1}$) or a
93 constant-current, four-probe method ($\sigma > 10 (\Omega \text{ cm})^{-1}$). We note that v_f and σ were the
94 only quantities measured in these experiments.

95 To estimate the T and ρ of the sample in the peak state two different EOS models for hy-
96 drogen and deuterium were considered; a tabular EOS denoted as Kerley²⁴ and an analytical
97 EOS denoted as Ross.^{25–27} Because only one of these EOS models (Kerley) was in a tabular
98 format, conducive for use in hydrodynamic simulations, two different methods were used to
99 infer T and ρ ; these two methods were described by NWM as being different but equivalent.
100 Method 1, used for the Kerley EOS, inferred T and ρ from hydrodynamic simulations of
101 the impact experiments, and therefore fully accounted for the multiple-shock nature of the
102 experiments. Method 2, used for the Ross EOS, inferred T and ρ by determining $T(P_{\text{max}})$
103 and $\rho(P_{\text{max}})$ along an isentrope centered at the first shocked state of the hydrogen or deu-
104 terium (P_1 , T_1 , and ρ_1), where P_{max} was the peak P reached in the experiment. In other
105 words, method 2 only accounted for the entropy increase due to the first shock, and treated
106 the subsequent compression as isentropic.

107 These two methods are, in fact, not equivalent; method 2 fails to account for the non-
108 negligible increase in entropy that results from the subsequent shocks during the reverbera-
109 tion. The difference in these two methods is illustrated in Fig. 2, which shows two different
110 hydrodynamic simulations using the same EOS for hydrogen, Kerley03,²⁸ a modern revision
111 of the Kerley EOS used by NWM. The red line represents a simulation accounting for the
112 full multiple-shock nature of the experiments (method 1). The blue line represents a simu-

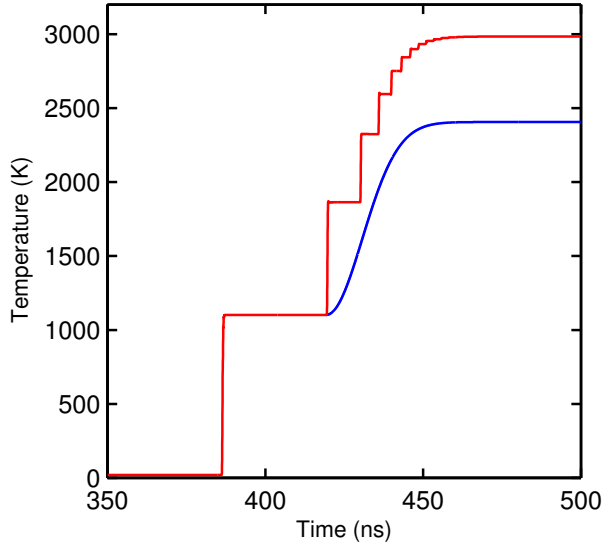


FIG. 2. Comparison of the two methods used by NWM to infer T in the multiple-shock experiments on hydrogen and deuterium. Red line; hydrodynamic simulation accounting for the full multiple-shock nature of the experiment (in this case SLDM12-H₂). Blue line; hydrodynamic simulation with the same magnitude first shock followed by ramp compression to the same peak P (in this case 142 GPa). Both simulations used the Kerley03²⁸ EOS for hydrogen (a modern revision of the Kerley²⁴ EOS used by NWM).

113 lation with the same magnitude first shock followed by ramp compression to the same peak
 114 P (method 2). In these simulations EOS models 3325,^{29,30} 3700,^{31,32} and 7411³³ were used
 115 to model copper, aluminum, and sapphire, respectively. As can be seen in the figure, T in
 116 the peak state for these two simulations differs by over 500 K. This is completely explained
 117 by the difference in entropy of the final states for the two different methods used by NWM.
 118 As a result, the T in the peak states inferred by NWM using the Kerley EOS with method
 119 1 and the Ross EOS with method 2 were considerably different.

120 The differences in inferred T for the subset of hydrogen experiments performed by NWM
 121 are shown graphically in Fig. 3 and listed in Table I. The colors and symbols denote the
 122 method used to infer T and the EOS model, respectively: red and blue correspond to method
 123 1 and 2, respectively; squares, circles, and diamonds correspond to the Ross, Kerley, and
 124 Kerley03 EOS, respectively. As can be seen in Fig. 3 the largest difference in inferred T
 125 is due to the method used, not the EOS model. In particular, the red and blue diamonds
 126 represent inferred T for the same EOS model (Kerley03) using the two different methods

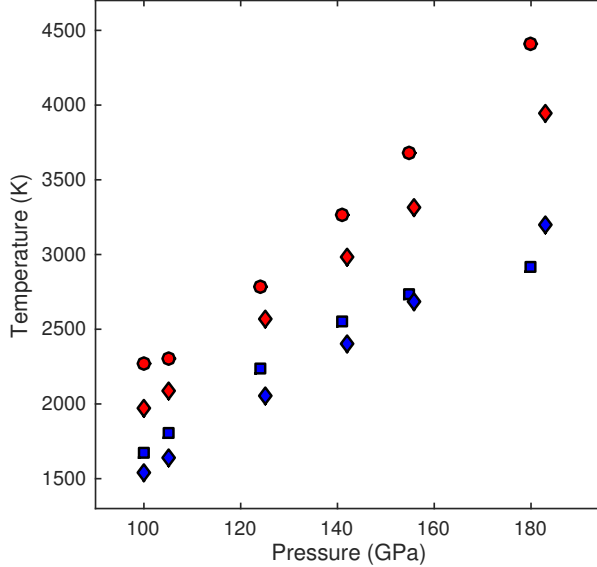


FIG. 3. Comparison of the inferred T for the NWM hydrogen experiments. The colors and symbols denote the method used to infer T and the EOS model, respectively: red and blue correspond to method 1 and 2, respectively; squares, circles, and diamonds correspond to the Ross,^{25–27} Kerley,²⁴ and Kerley03²⁸ EOS, respectively.

127 outlined above. The T difference ranges from ~ 440 - 750 K (~ 20 - 30%) with an average T
 128 difference of ~ 550 K over the entire P range. In contrast, differences in inferred T between
 129 various models for the same calculation method are noticeably smaller.

130 NWM interpreted the large T difference arising from the two calculation methods as
 131 being due to differences in the Kerley and Ross EOS models with respect to dissociation.
 132 They concluded that the Kerley EOS neglected dissociation at the conditions reached in
 133 their experiments, and therefore resulted in higher inferred T as compared to the Ross EOS.
 134 They therefore chose to use the T and ρ values inferred from the Ross EOS (using method
 135 2) to estimate the states reached in their experiments. However, due to the error in method
 136 2, these conditions do not accurately reflect the T states reached. We contend that the T
 137 obtained by method 1 using the Kerley03 EOS are a better representation. We note that
 138 a similar analysis performed with a revised EOS for hydrogen and deuterium by Saumon³⁴
 139 resulted in very similar T and ρ states (see Table I), lending confidence in these inferred
 140 values. Also, we note that Kerley03 is a widely-used EOS model and was used to infer T
 141 and ρ (along with the vdW-DF2 xc functional) in the low- T , high- ρ metallization study.¹⁵
 142 Finally, we acknowledge that EOS models based on FT-DFT calculations are available.^{35,36}

TABLE I. Inferred P , T , and ρ states reached in the multiple-shock experiments^{21,22} on hydrogen and deuterium performed by NWM. The first four columns list the experiment designation, impactor material, measured impact velocity, and measured σ , respectively. The subsequent columns list the inferred P , T , and ρ reported by NWM (using the Ross EOS and method 2) and the inferred P , T , and ρ obtained using method 1 and the Kerley03²⁸ and Saumon³⁴ EOS. The subsequent analysis performed in this work uses the values inferred from the Kerley03 EOS.

Experiment	Impactor	v_f (km/s)	σ ($\Omega \text{ cm}^{-1}$)	NWM			Kerley03			Saumon		
				P (GPa)	T (K)	ρ (g/cm ³)	P (GPa)	T (K)	ρ (g/cm ³)	P (GPa)	T (K)	ρ (g/cm ³)
SLDMS4-D ₂	Aluminum	5.59	0.71	93	2090	1.17	93	2204	1.25	93	2197	1.26
SLDMS5-D ₂	Aluminum	6.76	77	121	2760	1.29	121	2987	1.38	121	2998	1.39
SLDMS8-D ₂	Aluminum	7.33	417	135	3090	1.35	136	3397	1.44	136	3476	1.45
SLDMS6-H ₂	Aluminum	5.90	2.6	100	1670	0.61	100	1978	0.64	100	1867	0.66
SLDMS13-H ₂	Aluminum	6.10	7.1	105	1810	0.62	105	2093	0.66	105	1976	0.67
SLDMS7-H ₂	Aluminum	6.90	135	124	2230	0.66	125	2567	0.70	125	2430	0.72
SLDMS9-H ₂	Aluminum	6.91	313	124	2230	0.66	125	2573	0.70	125	2436	0.72
SLDM12-H ₂	Copper	5.58	2380	141	2560	0.69	142	2984	0.73	142	2889	0.76
SLDMS10-H ₂	Copper	5.96	1670	155	2730	0.72	156	3310	0.76	156	3253	0.79
SLDMS11-H ₂	Copper	6.65	2000	180	2910	0.77	183	3951	0.81	183	3848	0.84

143 However, at the P , T , and ρ conditions relevant here these models rely primarily on FT-
144 DFT calculations using the PBE⁸ xc functional. As shown here and elsewhere,^{1,7} PBE
145 systematically underestimates the P conditions necessary for dissociation, which can result
146 in isentropes that exhibit $-dT/dP$ at P below where saturation in σ was observed in the
147 NWM experiments. Perhaps even more problematic, we show in Sec. IV that PBE exhibits
148 P errors that result in calculated P that are too low at a given T and ρ condition, or
149 equivalently, ρ that are too high at a given P and T condition. For these reasons we do
150 not consider these PBE based EOS tables in estimating the conditions reached in the NWM
151 experiments.

152 To infer an energy gap as a function of ρ from their measurements of σ , NWM appealed
153 to a simplified semiconductor model. The data were fit to

$$\sigma = \sigma_0 \exp \left[- E_g(\rho)/2k_B T \right] \quad (1)$$

154 where σ_0 is the limiting value of conductivity, k_B is Boltzmann's constant, and $E_g(\rho)$ is the
155 energy gap, assumed to be linear in ρ and independent of T . The result of a least-squares

156 fit was reported to be

$$E_g(\rho) = 20 - 62.6\rho \quad (2)$$

157 where E_g is in units of eV, ρ is the molar density in units of mol/cm³, and $\sigma_0 = 90$ (Ω cm)⁻¹.
 158 NWM suggested this fit was reasonable, noting that a value of $\sigma_0 = 200 - 300$ (Ω cm)⁻¹ is
 159 typical of liquid semiconductors. However, this value for the limiting conductivity requires a
 160 negative energy gap to reproduce the measured σ for molar densities above ~ 0.32 mol/cm³
 161 (using the Ross EOS and method 2 to infer ρ), which is inconsistent with the requirement
 162 that $E_g \geq 0$. If one uses the same model, but instead constrains σ_0 to be the average of the
 163 measured σ at saturation, $\sigma_0 = 1850$ (Ω cm)⁻¹, a physically reasonable result is obtained.
 164 In this case

$$E_g(\rho) = 18.3 - 49.8\rho \quad (3)$$

165 and the gap closes at ~ 0.37 mol/cm³ (using the Kerley03 EOS and method 1 to infer ρ),
 166 consistent with the observed saturation in σ .

167 These two fits are displayed graphically in Fig. 4(a). The black and gray circles are the
 168 energy gap values obtained from Eq. 1 using the T and ρ values inferred from the Ross EOS
 169 using method 2 and the T and ρ values inferred from the Kerley03 EOS using method 1,
 170 respectively. The dashed and solid black lines are the corresponding fits (Eq. 2 and Eq. 3,
 171 respectively). The dashed gray line denotes the temperature of the system in eV ($k_B T$ as a
 172 function of ρ). This figure clearly shows the inconsistent behavior that arises from setting
 173 the limiting conductivity value at $\sigma_0 = 90$ (Ω cm)⁻¹. The estimated energy gap reaches a
 174 value equal to ($k_B T$) at ~ 0.32 mol/cm³, significantly lower than the ρ at which a minimum
 175 metallic conductivity was reached in the experiments. In order to match the measured σ
 176 at higher ρ a negative energy gap is required. The more reasonable value of $\sigma_0 = 1850$
 177 (Ω cm)⁻¹ results in an energy gap that is systematically larger by ~ 2 eV, reaching zero at
 178 ~ 0.37 mol/cm³, in agreement with observations.

179 We note that ρ was not measured in the experiments performed by NWM; the quantity in
 180 the peak state that was most tightly constrained is the peak P . We therefore also considered
 181 the inferred energy gap as a function of P , as shown in Fig. 4(b). Again, the estimated energy
 182 gap using the T and ρ values inferred by NWM using $\sigma_0 = 90$ (Ω cm)⁻¹ is systematically low,
 183 reaching a value equal to ($k_B T$) at ~ 120 GPa, roughly 20 GPa lower than the P at which
 184 a minimum metallic conductivity was reached in the experiments. However, because of the

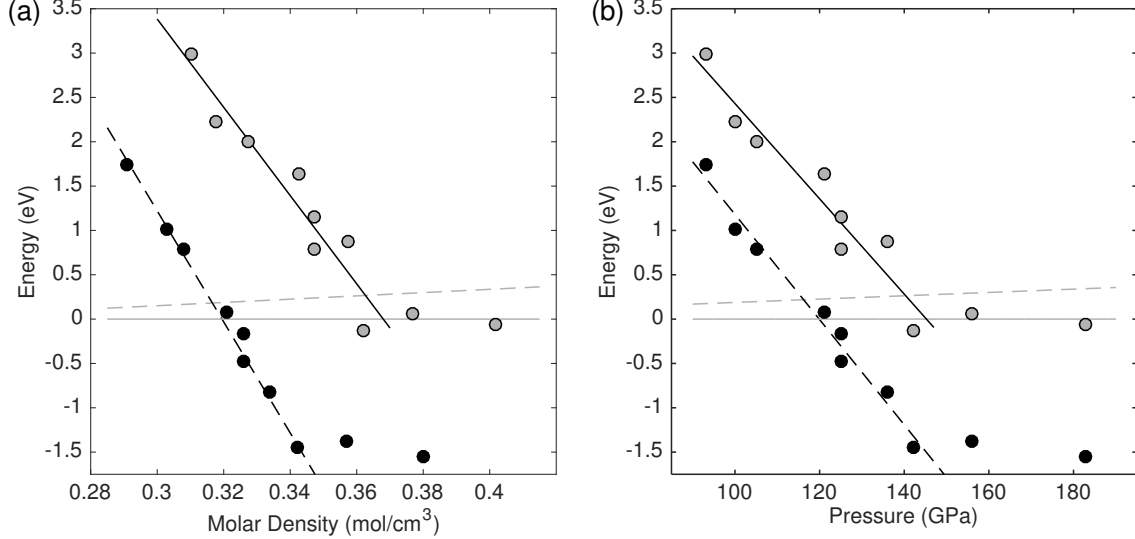


FIG. 4. Energy gap as a function of (a) molar density and (b) P . The black and gray circles are the energy gap values obtained from Eq. 1 using $\sigma_0 = 90 \text{ } (\Omega \text{ cm})^{-1}$ with T and ρ values inferred from the Ross^{25–27} EOS using method 2 and those obtained from Eq. 1 using $\sigma_0 = 1850 \text{ } (\Omega \text{ cm})^{-1}$ with T and ρ values inferred from the Kerley03²⁸ EOS using method 1, respectively. The dashed and solid black lines are the corresponding fits (Eq. 2 and Eq. 3, respectively). The dashed gray line denotes the temperature of the system in eV ($k_B T$ as a function of ρ or P).

185 difference in inferred ρ between the Ross and Kerley03 EOS, the systematic difference in the
 186 energy gap when viewed as a function of P is ~ 1 eV. Thus the error in the NWM fit to the
 187 semiconductor model (with $\sigma_0 = 90 \text{ } (\Omega \text{ cm})^{-1}$) underestimates the energy gap by ~ 1 eV as
 188 a function of P as compared to the same semiconductor model with a more reasonable value
 189 of σ_0 . In the subsequent section we will compare the results of first-principles simulations
 190 to this semiconductor model.

191 III. COMPARISON WITH FIRST-PRINCIPLES CALCULATIONS

192 First-principles (FP) calculations of the electrical conductivity (σ) and the energy gap
 193 at conditions consistent with the multiple-shock compression experiments^{21,22} performed by
 194 NWM were carried out within the framework of finite temperature density functional theory
 195 (FT-DFT). Both semi-local (PBE⁸) and nonlocal (vdW-DF1⁹ and vdW-DF2¹⁰) exchange
 196 and correlation (xc) functionals were considered. FP molecular dynamics simulations were

197 performed using the Vienna *ab initio* simulation package (VASP), a plane-wave DFT code
 198 developed at the Technical University of Vienna.^{37–39} The density was fixed by the total
 199 volume of the cubic supercell and the ion temperature was regulated with a Nosé-Hoover
 200 thermostat.^{40–42} A total 256 atoms were included in the supercell, with a plane-wave cutoff
 201 energy of 1200 eV. Simulations were performed in the canonical ensemble, and typically
 202 covered a few to several picoseconds of real time. The thermodynamic quantities were taken
 203 as averages over an equilibrated portion of the cumulative averages.

204 The electrical conductivity was calculated by averaging over 40 randomly selected
 205 snapshots for a given temperature (T) and density (ρ) configuration using the Kubo-
 206 Greenwood^{43,44} formula

$$\sigma(\omega) = \frac{2\pi e^2}{3Vm_e^2\omega} \sum_{\mathbf{k}\nu\mu} |\langle \mathbf{k}\nu | \hat{\mathbf{p}} | \mathbf{k}\mu \rangle|^2 (f_{\mathbf{k}\nu} - f_{\mathbf{k}\mu}) \delta(E_{\mathbf{k}\mu} - E_{\mathbf{k}\nu} - \hbar\omega), \quad (4)$$

207 where ω is the frequency, V is the volume of the supercell, e and m_e are the charge and mass
 208 of electrons, respectively, and $f_{\mathbf{k}\mu}$ is the Fermi occupation number for a given temperature.
 209 The eigenvalues $E_{\mathbf{k}\mu}$ for the Bloch states $|\mathbf{k}\mu\rangle$ are computed within each step of the FT-DFT
 210 simulation so that the dipole matrix elements $\langle \mathbf{k}\nu | \hat{\mathbf{p}} | \mathbf{k}\mu \rangle$ are determined with the momentum
 211 operator. The imaginary part of the electrical conductivity can be obtained from a Kramers-
 212 Kronig transformation. For these calculations the Brillouin zone was sampled by a $5 \times 5 \times 5$
 213 Monkhorst-Pack \mathbf{k} -point grid.⁴⁵

214 The density of states (DOS) was obtained from the same set of 40 randomly selected
 215 snapshots. For each given T and ρ configuration a histogram of the eigenvalues of the
 216 band energies was created from the collection of snapshots and smoothed with a gaussian of
 217 width 0.2 eV. The energy gaps were extracted directly from the simulations. For each time
 218 step eigenvalues in the vicinity of the fermi energy were extracted. These eigenvalues were
 219 then averaged. The energy gap was obtained from the energy difference of the averaged
 220 eigenvalues. The precision to which the energy gap can be directly computed from the
 221 simulations is set by the local separation of eigenvalue energies on either side of the gap.
 222 Eigenvalue averages for adjacent eigenstates indicate these local differences to be ~ 0.15 eV;
 223 states with energy gap values on the order of 0.15 eV or less were assumed to be have a
 224 closed gap and the energy gap was set to zero.

225 As described in Sec. II, the measured quantities in the multiple-shock experiments of
 226 NWM were the impact velocity (v_f) and σ . The peak P in the experiment was determined

227 from the measured v_f and the known EOS of the impactor (copper or aluminum), baseplate
 228 (aluminum), and anvils (sapphire). In the reverberation geometry used in these experiments
 229 the P in the peak state is independent of the EOS of hydrogen or deuterium, and is therefore
 230 well constrained. In contrast, T and ρ in the peak state are calculated and are therefore
 231 dependent upon the particular model used for hydrogen or deuterium. For the reasons
 232 discussed in Sec. II, we used the Kerley03²⁸ EOS to estimate the T and ρ conditions at the
 233 corresponding peak P (see Table II).

234 To perform a detailed comparison of the NWM experiments with FP calculations we first
 235 had to determine how best to equate the peak state of the system. In general, the EOS
 236 surface of different models are not coincident. Thus, in comparing two models one can only
 237 match two of the three variables P , T , and ρ that define a particular state of the system.
 238 Since the peak P in these experiments does not depend upon the hydrogen or deuterium
 239 EOS, P is an obvious choice for one of the variables to equate. The second variable to
 240 equate is less obvious. However, in exploring the EOS surface it was found that in this P ,
 241 T , and ρ regime P depends much more strongly on ρ than T . For example, at ~ 100 GPa
 242 a $\sim 10\%$ increase in P required only a $\sim 5\%$ increase in ρ , while the same increase in P
 243 required roughly a factor of two increase in T . Thus for the comparisons presented here, T
 244 is a more appropriate second variable to equate than ρ . We therefore chose to fix the T in
 245 the FT-DFT simulations and vary the ρ until the experimentally inferred P was reached.

246 The resulting P , T , and ρ states obtained in this way using PBE, vdW-DF1, and vdW-
 247 DF2 xc functions are listed in Table II (for each functional P and T are the same as those
 248 listed under Kerley03). As expected, systematic differences in the inferred ρ were observed.
 249 In particular, the ρ inferred using the PBE xc functional were found to be significantly larger
 250 ($\sim 9\text{-}12\%$) than the values obtained from Kerley03. In contrast, both of the nonlocal vdW
 251 xc functionals resulted in ρ values that were in better agreement with the Kerley03 EOS.
 252 For both functionals the ρ was found to be lower than Kerley03 at low P (-0.1% and -2.2%
 253 for vdW-DF1 and vdW-DF2, respectively) and higher than Kerley03 at high P ($+5.4\%$ and
 254 $+2.1\%$ for vdW-DF1 and vdW-DF2, respectively). These ρ differences and their effect on
 255 the calculated σ will be discussed in more detail in the next section.

256 The calculated σ for the various xc functionals at these P , T , and ρ conditions are listed
 257 in Table II and plotted as a function of P in Fig. 5(a). This comparison suggests that PBE
 258 significantly overestimates σ in this P , T , and ρ regime. In particular, calculations using the

TABLE II. Predicted σ from various xc functionals for the estimated P , T , and ρ states reached in the multiple-shock experiments^{21,22} on hydrogen and deuterium performed by NWM. The first two columns list the experimental designation and the measured σ , respectively. The next three columns list the T , P , and ρ states reached as inferred using the Kerley03²⁸ EOS. The subsequent columns list the predicted σ and ρ at the inferred P and T for the PBE, vdW-DF1, and vdW-DF2 xc functionals.

Experiment	σ ($\Omega \text{ cm}^{-1}$)	Kerley03			PBE		DF1		DF2	
		P (GPa)	T (K)	ρ (g/cm^3)	σ ($\Omega \text{ cm}^{-1}$)	ρ (g/cm^3)	σ ($\Omega \text{ cm}^{-1}$)	ρ (g/cm^3)	σ ($\Omega \text{ cm}^{-1}$)	ρ (g/cm^3)
SLDMS4-D ₂	0.71	93	2204	1.25	4989	1.397	1.99	1.249	0.30	1.222
SLDMS5-D ₂	77	121	2987	1.38	8919	1.534	4518	1.437	493	1.359
SLDMS8-D ₂	417	136	3397	1.44	9970	1.589	5461	1.514	3234	1.455
SLDMS6-H ₂	2.6	100	1978	0.64	3456	0.710	0.62	0.641	0.11	0.624
SLDMS13-H ₂	7.1	105	2093	0.66	4990	0.729	2.32	0.652	0.35	0.636
SLDMS7-H ₂	135	125	2567	0.70	9034	0.780	1546	0.722	16.2	0.683
SLDMS9-H ₂	313	125	2573	0.70	9034	0.781	1546	0.722	16.2	0.683
SLDM12-H ₂	2380	142	2984	0.73	10410	0.816	5671	0.777	1693	0.737
SLDMS10-H ₂	1670	156	3310	0.76	11290	0.840	7061	0.807	3880	0.774
SLDMS11-H ₂	2000	183	3951	0.81	13180	0.881	8907	0.854	6551	0.827

259 PBE xc functional predict that a minimum metallic conductivity should have been observed
260 in all experiments performed by NWM. In contrast, the overall trend of the experimental
261 data is captured reasonably well by the two nonlocal vdW functionals. However, when
262 σ is plotted as a function of molar density, as in Fig. 5(b), all three functionals appear
263 to adequately reproduce the experimental results. In particular, the predicted σ for the
264 two sets of calculations (hydrogen and deuterium) collapse onto linear trend lines in $\log(\sigma)$
265 vs. ρ (dashed lines in Fig. 5). These trend lines are systematically offset by one order
266 of magnitude in σ . We note that given the higher shock impedance of deuterium, those
267 experiments reached ~ 400 K higher T at a similar P and molar density as compared to
268 hydrogen. These isotopic differences will be explored further in the next section.

269 Similar behavior is exhibited in the inferred energy gaps extracted from FP calculations
270 of the DOS. Figure 6 shows the calculated DOS for the conditions reached in the subset of
271 hydrogen experiments performed by NWM. Energy gap values obtained for the various xc
272 functionals at the T and ρ conditions listed in Table II are plotted in Fig. 7 as functions

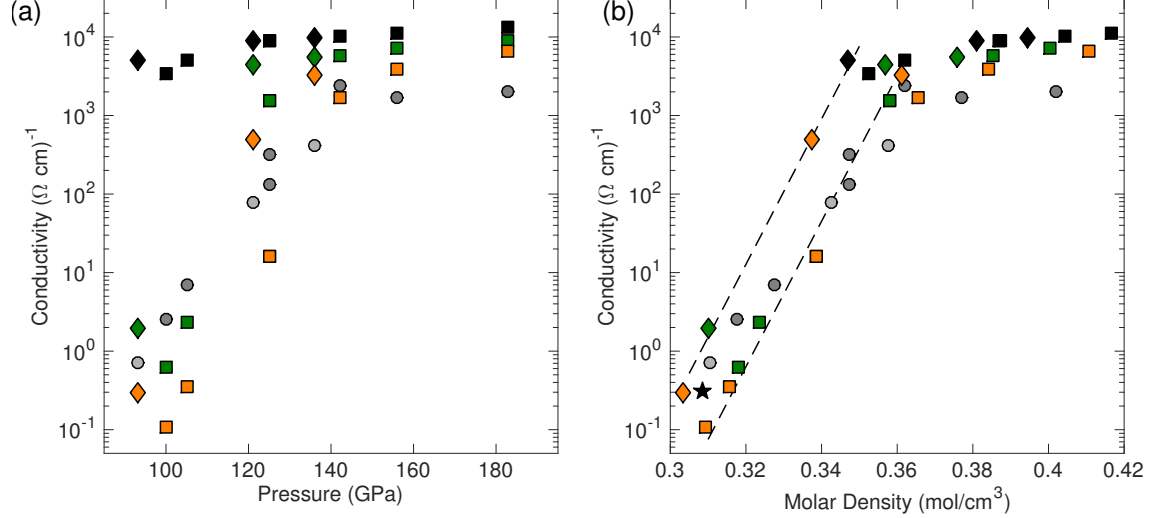


FIG. 5. Conductivity as a function of (a) P and (b) molar density. Dark (light) gray circles, measured^{21,22} σ for hydrogen (deuterium); Black, green, and orange squares (diamonds), calculated σ of hydrogen (deuterium) using PBE,⁸ vdW-DF1⁹, and vdW-DF2¹⁰ xc functionals, respectively, at the conditions listed in Table II. The black star is an additional calculated conductivity using PBE at a lower molar density described in Sec. IV. Dashed lines in (b) are guides to the eye that are offset by one order of magnitude in σ .

273 of both P and molar density. Also shown in the figure for reference are the inferred energy
 274 gap values obtained from the measured σ using Eq. 1 with $\sigma_0 = 1850 (\Omega \text{ cm})^{-1}$ and the
 275 T and ρ values inferred from the Kerley03 EOS. As was the case for σ , PBE appears to
 276 significantly underestimate the energy gap in this P , T , and ρ regime, while the nonlocal
 277 vdW functionals are in reasonable agreement with the energy gap values inferred from the
 278 simple semiconductor model described in Sec. II. However, again, when viewed as a function
 279 of molar density, all three functionals appear to exhibit very similar results; the extracted
 280 energy gaps for the two sets of calculations (hydrogen and deuterium) collapse onto linear
 281 trend lines (dashed lines in Fig. 7). These trend lines are offset in energy, with the deuterium
 282 trend line being systematically ~ 1 eV lower than that of hydrogen. Again, these isotopic
 283 differences will be explored further in the next section.

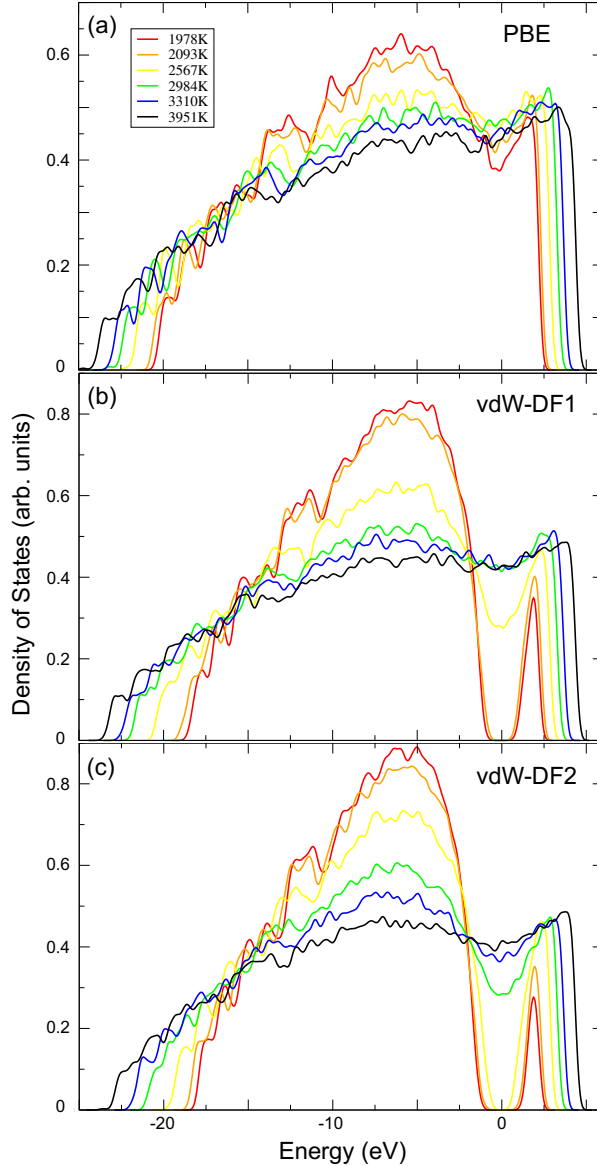


FIG. 6. Density of states extracted from FP calculations for (a) PBE, (b) vdW-DF1, and (c) vdW-DF2 at the P , T , and ρ conditions (listed in Table II) reached in the multiple-shock experiments^{21,22} on hydrogen performed by NWM.

284 IV. DISCUSSION

285 The comparisons shown in Figs. 5 and 7 suggest that the most important parameter in
 286 determining the location of the MA transition for the various xc functionals is the molar
 287 density, at least in this P , T , and ρ regime. Given this observation, and the significantly
 288 larger ρ predicted by PBE at the P and T conditions considered here, one must ask the

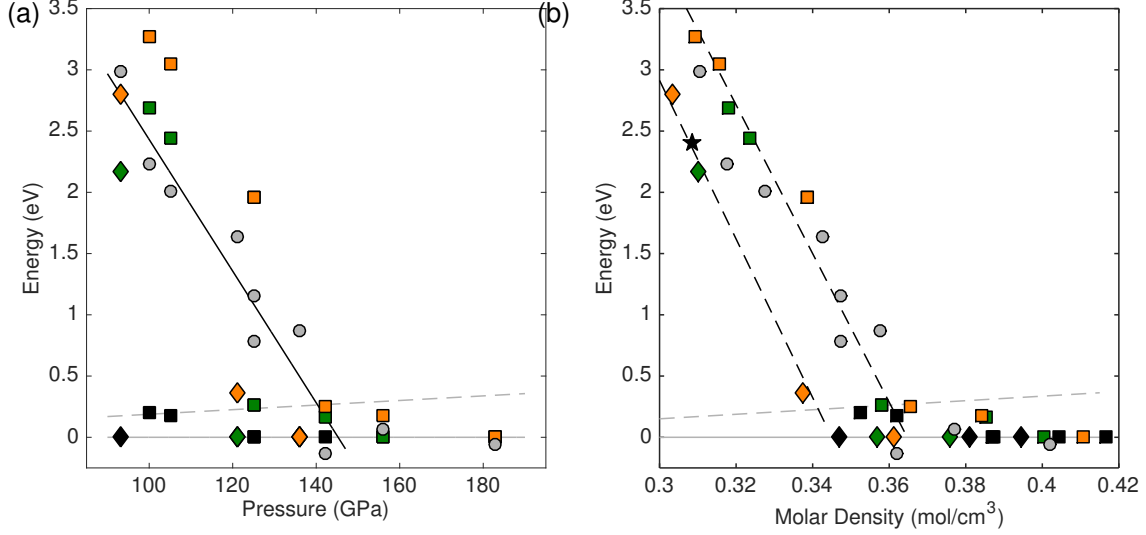


FIG. 7. Energy gap as a function of (a) P and (b) molar density. The gray circles are the energy gap values obtained from Eq. 1 using $\sigma_0 = 1850 \text{ } (\Omega \text{ cm})^{-1}$ with the T and ρ values inferred from the Kerley03²⁸ EOS (see Table II). The dashed gray line denotes the temperature of the system in eV ($k_B T$ as a function of P or ρ); the solid black line is a fit to data where the inferred gap was greater than the temperature of the system. Black, green, and orange squares (diamonds), calculated energy gap of hydrogen (deuterium) using PBE,⁸ vdW-DF1⁹, and vdW-DF2¹⁰ xc functionals, respectively, at the conditions listed in Table II. The black star is an additional calculated energy gap using PBE at a lower molar density described in Sec. IV. Dashed lines in (b) are guides to the eye and indicate an offset of ~ 1 eV between hydrogen and deuterium.

289 question whether the comparison of the NWM experiments with PBE are biased by our
 290 choice to equate the P and T in the peak state as opposed to the P and ρ . To investigate
 291 this we performed several more FP calculations of experiment SLDMS13-H₂ (one of the
 292 lower P hydrogen experiments) using the PBE xc functional.

293 Fixing the T and ρ at 2093 K and 0.66 g/cm^3 (conditions estimated by the Kerley03 EOS)
 294 results in a P of 88 GPa for the PBE xc functional, $\sim 16\%$ lower than the experimentally
 295 inferred P of 105 GPa. An increase of $\sim 10\%$ in ρ (to 0.729 g/cm^3) was required to increased
 296 the P to 105 GPa. These were the P , T , and ρ values used in the calculations described in
 297 the previous section (see Table II). Here, we instead fixed the ρ at 0.66 g/cm^3 and varied
 298 the T . A T increase to 5800 K (a factor of ~ 2.8) was required to match the experimentally
 299 inferred P of 105 GPa. The resulting state was found to exhibit metallic behavior, with σ

300 = 7500 ($\Omega \text{ cm}$)⁻¹ and no energy gap. We performed a similar exercise at an intermediate ρ
 301 of 0.689 g/cm³. In this case, a T increase to 4200 K (a factor of ~ 2) was required to reach
 302 the experimentally inferred P of 105 GPa. Again, this state was found to exhibit metallic
 303 behavior, with $\sigma = 7600$ ($\Omega \text{ cm}$)⁻¹ and no energy gap. It seems clear that for the PBE
 304 xc functional no matter what T and ρ combination one uses to match the experimentally
 305 inferred P of 105 GPa, the calculated σ will be much too high, by roughly three orders of
 306 magnitude. The same conclusions would be reached for the higher P experiments performed
 307 by NWM. From this exercise we conclude that regardless of how one tries to equate the
 308 P states reached in the NWM experiments, predictions using the PBE xc functional are
 309 inconsistent with the measured σ .

310 To further explore the trends observed in σ and energy gap with molar density, we also
 311 performed calculations with the PBE xc functional at lower P . The Kerley03 EOS was used
 312 to estimate the T that would be reached in a ~ 80 GPa multiple-shock experiment. These P
 313 and T conditions, 80 GPa and 1500 K, respectively, correspond to a molar density of 0.3085
 314 g/cm³ with the PBE xc functional. At these conditions PBE predicts $\sigma = 0.31$ ($\Omega \text{ cm}$)⁻¹ and
 315 an energy gap of 2.4 eV (shown as black stars in Figs. 5(b) and 7(b)). While these result
 316 do reasonably follow the trends exhibited by the nonlocal vdW xc functionals, PBE does
 317 appear to display gap closure at a slightly lower molar density. However, we note the T for
 318 this PBE calculation is considerably lower (1500 K) than the other calculations considered
 319 here.

320 To evaluate the relative effect of T on the FP calculations we consider σ as a function of
 321 band gap energy, shown in Fig. 8. The as calculated values (listed in Table II) are plotted
 322 in Fig. 8(a). Also plotted as triangles and squares are the experimentally measured σ as
 323 a function of inferred energy gap as determined by NWM and reanalyzed in this work,
 324 respectively; dark and light gray correspond to hydrogen and deuterium, respectively. As
 325 expected, the FP calculations, particularly with the nonlocal vdW xc functionals, are in
 326 reasonable agreement with the experimental measurements and the reanalyzed energy gaps,
 327 showing a small scatter about a common trend line. These σ values were then normalized to
 328 a common T of 1978 K (the lowest inferred experimental T) using the semiconductor model:

$$\sigma_n = \sigma_1 \exp \left[\frac{-E_{g_1}}{2k_B T_1} \left(\frac{T_1}{1978} - 1 \right) \right] \quad (5)$$

329 where σ_1 at T_1 and E_{g_1} has been normalized to σ_n at T of 1978 K and the same energy

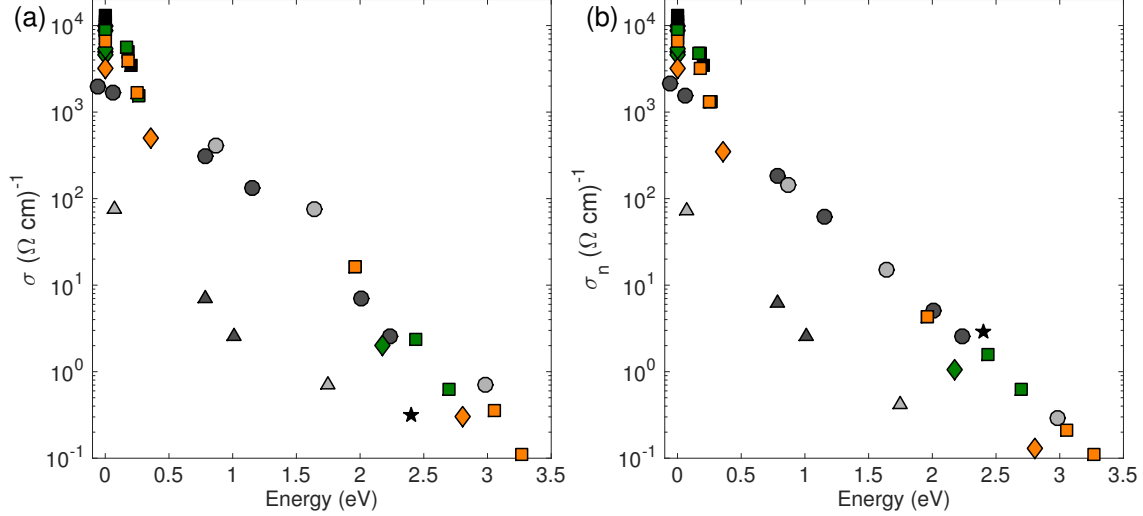


FIG. 8. Conductivity as a function of energy gap. (a) Dark and light gray circles (triangles) are the results for hydrogen and deuterium, respectively, from experiments^{21,22} performed by NWM where the energy gap was inferred from the modified (original) semiconductor model described in Sec. II. Black, green, and orange squares (diamonds) are calculations for hydrogen (deuterium) using PBE,⁸ vdW-DF1⁹, and vdW-DF2¹⁰ xc functionals, respectively, at the conditions listed in Table II. The black star is the additional PBE calculation performed at lower molar density. (b) Same as (a) but with the conductivity values normalized (Eq. 5) to a common T (1978 K, corresponding to the lowest T NWM experiment) as described in the text.

330 gap E_{g1} . The normalized experimental and calculated σ_n are plotted as a function of energy
 331 gap in Fig. 8(b). We see that the small scatter apparent in Fig. 8(a) can be explained by
 332 the corresponding T differences. In particular, the low value for σ obtained for the 1500 K
 333 PBE calculation is largely due to the correspondingly low thermal excitation. These results
 334 do suggest a small isotopic difference for FP calculations of hydrogen and deuterium; σ
 335 for deuterium appears to be systematically lower than that of hydrogen by a factor of 2-3.
 336 While the source of this small isotopic difference is not entirely clear, it suggests the energy
 337 gap is both a function of T and ρ in this regime, as one might expect.

338 These comparisons suggest that the significant differences in σ and the energy gap exhib-
 339 ited by the various xc functionals when viewed as a function of P , as in Figs. 5(a) and 7(a),
 340 are largely tied to differences in the predicted P for the xc functionals at similar T and ρ
 341 conditions. We note that the various functionals considered here have recently been care-

342 fully evaluated with respect to quantum Monte Carlo (QMC) calculations by Clay *et al.*⁴⁶
343 They explored the accuracy of the various functionals in comparison to QMC calculations
344 for both liquid and solid hydrogen structures. The vdW functionals, particularly vdW-DF1,
345 were found to provide a very good description of the global and local energetics as compared
346 to QMC, but exhibited larger differences in P than PBE relative to the QMC calculations.
347 The P obtained from all of the xc functionals were higher than QMC (by $\sim 5-10\%$ in the
348 relevant ρ regime), with PBE and vdW-DF2 being the lowest and highest, respectively.

349 This trend in P differences observed by Clay *et al.*, which is consistent with the trend
350 observed in this study, would seem to suggest that the P determined by the vdW functionals
351 is too high rather than the P determined by PBE being too low. However, this conclusion is
352 refuted by the incompatibility of PBE with the measured σ from the NWM experiments. We
353 note that the calculations by Clay *et al.* were carried out in liquid structures with Wigner-
354 Seitz radii (r_s) of 1.30, 1.45, and 1.60 (1.23, 0.88, and 0.66 g/cm³ in hydrogen, respectively)
355 at $T = 1000$ K. The ρ range considered here corresponds to an r_s of 1.5-1.6, within the
356 range evaluate by Clay *et al.*, however, the T range considered here (2-4 kK) is higher. At
357 higher T , thermal population of electrons into the excited states is not insignificant. This
358 thermal occupation of electronic orbitals has direct consequences on the liquid structure and
359 the forces, but is not included in the QMC calculations.

360 Similar observations were made in a recent evaluation of the various xc functionals with
361 high-precision Hugoniot and reshock measurements on liquid deuterium,⁷ which probed the
362 MA transition in the largely T -driven regime. In that study the same trend in P was
363 observed for the MA transition along the Principal Hugoniot; dissociation, as evidenced by
364 a transient drop in the slope of the shock velocity relative to the particle velocity behind the
365 shock front, occurred at a lower P for PBE than for the vdW functionals. Furthermore, the
366 experimentally determined P onset of dissociation was found to be bounded from below by
367 PBE (~ 3 GPa lower than experiment) and above by the vdW functionals (~ 1 GPa higher
368 than experiment). This conclusion was corroborated by measurements of the reshock P
369 from Hugoniot states near peak compression. Those measurements suggest that the reshock
370 P determined by the vdW functionals are too low by a few percent. In contrast, the P
371 difference for vdW-DF1 relative to QMC at those conditions is on the order of $+2-4\%$.
372 Again, while the trend in P was found to be the same as that determined by Clay *et al.*,
373 comparison with the MA transition along the Hugoniot suggests that the P for dissociation

374 is in better agreement with the vdW xc functionals, and that PBE underestimates the P
375 necessary for dissociation.

376 Finally, we note that there are conflicting experimental results for the MA transition in
377 the low- T , high- ρ regime where the transition appears to be largely ρ -driven (see Fig. 1).
378 Dynamic compression experiments¹⁵ on liquid deuterium in the ~ 1 -2 kK regime performed
379 at the Sandia Z machine revealed an abrupt MA transition, as evidenced by a rapid increase
380 in reflectivity, between ~ 280 and 305 GPa. Similar to the T -driven regime probed by the
381 Hugoniot and the intermediate regime probed by the σ measurements of NWM, the dynamic
382 compression experimental results are in reasonable agreement with the nonlocal vdW xc
383 functionals, and suggest that the PBE xc functional underestimates the P onset of the MA
384 transition. In contrast, static high- P and pulsed heated experiments¹⁷⁻²⁰ on hydrogen and
385 deuterium in a similar T regime suggest the MA transition occurs at ~ 75 to 170 GPa,
386 based on observation of T plateaus in the heating curves and increases in reflectivity, in
387 apparent agreement with PBE. However, these conditions are consistent with the onset of
388 strong optical absorption in the dynamic compression experiments, which lead to alternative
389 interpretations of those data.^{11,15,47} Furthermore, we have shown that the predictions of PBE
390 are inconsistent with the σ measurements of NWM. This raises questions about the static
391 high- P and pulsed heated studies, particularly given that the MA transition in those studies
392 is reported to be in a very similar P but even lower T range than the multiple-shock σ
393 experiments examined here.

394 V. CONCLUSION

395 A detailed comparison of the measured σ from multiple-shock compression experiments^{21,22}
396 with FT-DFT calculations using both semi-local (PBE) and nonlocal (vdW-DF1 and vdW-
397 DF2) xc functionals was performed. As a part of this comparison, the multiple-shock σ
398 experiments were reanalyzed; the original study included inconsistencies in both the inferred
399 T states reached in the experiments and in the fit to a semiconductor model used to inter-
400 pret the measured σ . Due to the method used to infer the T , which only accounted for the
401 entropy increase from the first shock and treated subsequent compression as isentropic, the
402 T states reported by NWM are systematically low by ~ 440 -750 K (~ 20 -30%). Also, due
403 to a low $\sigma_0 = 90$ (Ω cm)⁻¹, the energy gap inferred from a simple semiconductor model is

404 underestimated by ~ 1 eV as a function of P as compared to the same semiconductor model
405 with a more reasonable $\sigma_0 = 1850$ (Ω cm) $^{-1}$.

406 Using P and T conditions inferred from the Kerley03 EOS for the peak states, FP cal-
407 culations with PBE, vdW-DF1, and vdW-DF2 xc functionals were performed to directly
408 compare with the NWM experiments. Calculations of σ using the PBE xc functional predict
409 that a minimum metallic conductivity should have been observed in all of the experiments
410 performed by NWM. It was also shown that regardless of how one tries to equate the P
411 states reached in the NWM experiments, predictions using the PBE xc functional are in-
412 consistent with the measured σ . In contrast, the overall trend of the experimental data is
413 captured reasonable well by the two vdW xc functionals. Similar behavior was exhibited in
414 the inferred energy gaps extracted from FP calculations of the DOS.

415 This study, along with previous studies comparing the various xc functionals with recent
416 Hugoniot experiments⁷ on deuterium that probed the MA transition in the high- T and low- ρ
417 regime and dynamic compression experiments¹⁵ on deuterium that probed the MA transition
418 in the low- T and high- ρ regime, provides a consistent picture for the MA transition over a
419 wide P and T range. Over this entire range the P onset of the MA transition is captured
420 reasonably well by the nonlocal vdW xc functionals, while PBE appears to underestimate
421 the P conditions necessary for dissociation. This likely stems from P errors associated
422 with the PBE xc functional, resulting in calculated P that are too low at these T and ρ
423 conditions. This raises questions about recent static high- P and pulsed heated studies¹⁷⁻²⁰
424 that appear to be in agreement with predictions from PBE, particularly given that the MA
425 transition in those studies is reported to be in a very similar P but even lower T range than
426 the multiple-shock σ experiments examined here.

427 ACKNOWLEDGMENTS

428 This work was supported in part by the U.S. Department of Energy, National Nuclear
429 Security Administration under Award No. DE-NA0002007. Sandia National Laboratories is
430 a multimission laboratory managed and operated by National Technology and Engineering
431 Solutions of Sandia, LLC., a wholly owned subsidiary of Honeywell International, Inc., for
432 the U.S. Department of Energy's National Nuclear Security Administration under Contract
433 No. DE-NA0003525. This paper describes objective technical results and analysis. Any

434 subjective views or opinions that might be expressed in the paper do not necessarily represent
435 the views of the U.S. Department of Energy or the United States Government. MP and RR
436 thank the Deutsche Forschungsgemeinschaft (DFG) for support via the SFB 652.

437 * mknudson@wsu.edu

438 ¹ J. M. McMahon, M. A. Morales, C. Pierleoni, and D. M. Ceperley, *Rev. Mod. Phys.* **84**, 1607
439 (2012).

440 ² R. Smoluchowski, *Nature* **215**, 691 (1967).

441 ³ E. E. Salpeter, *Astrophys. J.* **181**, L83 (1973).

442 ⁴ W. Lorenzen, B. Holst, and R. Redmer, *Phys. Rev. B* **84**, 235109 (2011).

443 ⁵ T. Guillot, *Science* **286**, 72 (1999).

444 ⁶ N. Nettelmann, A. Becker, B. Holst, and R. Redmer, *Astrophys. J.* **750**, 52 (2012).

445 ⁷ M. D. Knudson and M. P. Desjarlais, *Phys. Rev. Lett.* **118**, 035501 (2017).

446 ⁸ J. P. Perdew, K. Burke, and M. Ernzerhof, *Phys. Rev. Lett.* **77**, 3865 (1996).

447 ⁹ M. Dion, H. Rydberg, E. Schröder, D. C. Langreth, and B. I. Lundqvist, *Phys. Rev. Lett.* **92**,
448 246401 (2004).

449 ¹⁰ K. Lee, E. D. Murray, L. Kong, B. I. Lundqvist, and D. C. Langreth, *Phys. Rev. B* **82**, 081101
450 (2010).

451 ¹¹ I. Tamblyn and S. A. Bonev, *Phys. Rev. Lett.* **104**, 065702 (2010).

452 ¹² M. A. Morales, C. Pierleoni, E. Schwegler, and D. M. Ceperley, *Proc. Natl. Acad. Sci. U.S.A.*
453 **107**, 12799 (2010).

454 ¹³ W. Lorenzen, B. Holst, and R. Redmer, *Phys. Rev. B* **82**, 195107 (2010).

455 ¹⁴ M. A. Morales, J. M. McMahon, C. Pierleoni, and D. M. Ceperley, *Phys. Rev. Lett.* **110**,
456 065702 (2013).

457 ¹⁵ M. D. Knudson, M. P. Desjarlais, A. Becker, R. W. Lemke, K. R. Cochrane, M. E. Savage,
458 D. E. Bliss, T. R. Mattsson, and R. Redmer, *Science* **348**, 1455 (2015).

459 ¹⁶ M. Matzen *et al.*, *Phys. Plasmas* **12**, 055503 (2005).

460 ¹⁷ V. Dzyabura, M. Zaghoo, and I. F. Silvera, *Proc. Natl. Acad. Sci. U.S.A.* **110**, 8040 (2013).

461 ¹⁸ K. Otha, K. Ichimaru, M. Einaga, S. Kawaguchi, K. Shimizu, T. Matsuoka, N. Hirao, and
462 Y. Ohishi, *Sci. Rep.* **5**, 16560 (2015).

- 463 ¹⁹ M. Zaghoo, A. Salamat, and I. F. Silvera, *Phys. Rev. B* **93**, 155128 (2016).
- 464 ²⁰ M. Zaghoo and I. F. Silvera, *Proc. Nat. Acad. Sci. U.S.A.* **114**, 11873 (2017).
- 465 ²¹ S. T. Weir, A. C. Mitchell, and W. J. Nellis, *Phys. Rev. Lett.* **76**, 1860 (1996).
- 466 ²² W. J. Nellis, S. T. Weir, and A. C. Mitchell, *Phys. Rev. B* **59**, 3434 (1999).
- 467 ²³ A. C. Mitchell and W. J. Nellis, *Rev. Sci. Instrum.* **52**, 347 (1981).
- 468 ²⁴ G. I. Kerley, “Molecular-based study of fluids,” (American Chemical Society, Washington,
469 1983) p. 107.
- 470 ²⁵ N. C. Holmes, M. Ross, and W. J. Nellis, *Phys. Rev. B* **52**, 15835 (1995).
- 471 ²⁶ M. Ross, *Phys. Rev. B* **54**, R9589 (1996).
- 472 ²⁷ M. Ross, *Phys. Rev. B* **58**, 669 (1998).
- 473 ²⁸ G. Kerley, Sandia National Laboratories Report No. SAND2003-3613 (Sandia National Labo-
474 ratories, 2003).
- 475 ²⁹ J. H. Carpenter, private communication (2014).
- 476 ³⁰ K. R. Cochrane, R. W. Lemke, Z. Riford, and J. H. Carpenter, *J. Appl. Phys.* **119**, 105902
477 (2016).
- 478 ³¹ G. I. Kerley, *Int. J. Impact Eng.* **5**, 441 (1987).
- 479 ³² G. Kerley, Kerley Publishing Services Report No. KPS98-1 (Kerley Publishing Services, 1998).
- 480 ³³ J. F. Barnes and S. P. Lyon, Los Alamos Technical Report No. LA-11058-MS (Los Alamos
481 National Laboratory, 1987).
- 482 ³⁴ D. Saumon, private communication (2018).
- 483 ³⁵ L. Caillabet, S. Mazevet, and P. Loubeyre, *Phys. Rev. B* **83**, 094101 (2011).
- 484 ³⁶ B. Holst, R. Redmer, and M. P. Desjarlais, *Phys. Rev. B* **77**, 184201 (2008).
- 485 ³⁷ G. Kresse and J. Hafner, *Phys. Rev. B* **47**, 558 (1993).
- 486 ³⁸ G. Kresse and J. Hafner, *Phys. Rev. B* **49**, 14251 (1994).
- 487 ³⁹ G. Kresse and J. Furthmüller, *Phys. Rev. B* **54**, 11169 (1996).
- 488 ⁴⁰ S. Nosé, *Mol. Phys.* **52**, 256 (1984).
- 489 ⁴¹ S. Nosé, *J. Chem. Phys.* **81**, 511 (1984).
- 490 ⁴² W. G. Hoover, *Phys. Rev. A* **31**, 1695 (1985).
- 491 ⁴³ R. Kubo, *J. Phys. Soc. Jpn.* **12**, 570 (1957).
- 492 ⁴⁴ D. A. Greenwood, *Proc. Phys. Soc.* **71**, 585 (1958).
- 493 ⁴⁵ H. J. Monkhorst and J. D. Pack, *Phys. Rev. B* **13**, 5188 (1976).

⁴⁹⁴ ⁴⁶ R. C. Clay, J. Mcminis, J. M. McMahon, C. Pierleoni, D. M. Ceperley, and M. A. Morales,
⁴⁹⁵ Phys. Rev. B **89**, 184106 (2014).

⁴⁹⁶ ⁴⁷ R. S. McWilliams, D. A. Dalton, M. F. Mahmood, and A. F. Goncharov, Phys. Rev. Lett. **116**,
⁴⁹⁷ 255501 (2016).